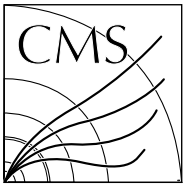

The Compact Muon Solenoid Experiment

CMS Note

Mailing address: CMS CERN, CH-1211 GENEVA 23, Switzerland

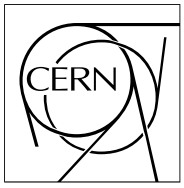

November 21, 2007

Tracking and Alignment with the Silicon Strip Tracker at the CMS Magnet Test Cosmic Challenge

D. Benedetti, M. Biasini, B. Caponeri, R. Covarelli

INFN & Università di Perugia, Italy

D. Britzger, M. Pioppi, R. Ranieri, F. J. Ronga

CERN, Geneva, Switzerland

N. Hadengue

EPFL, Lausanne, Switzerland

F. Palmonari

INFN & Università di Pisa, Italy

Abstract

Data were collected with a custom-built sub-structure of the silicon strip tracker, both during the preparation of the Magnet Test Cosmic Challenge and during the challenge itself. These data were used to evaluate performance of track reconstruction and detector alignment algorithms, both with and without magnetic field. The track reconstruction algorithm is described in detail and its performance presented, in terms of its efficiency, resolution and consistency with the results from other sub-detectors. A study of detector alignment is shown, including the use tracker construction information. The effect of alignment on track quality is discussed.

1 Introduction

During the Summer of 2006, the CMS collaboration, to prepare for the first data from proton-proton collisions, developed an exercise in which all the sub-detectors have for the first time worked together: the so-called **Magnet Test Cosmic Challenge** (**MTCC**). For the first time the performances of the detector were analysed in presence of a magnetic field varying from 0.0 to 4.0 Tesla. The goal of the exercise was the development of commissioning procedures and the detection of cosmic ray muons.

The silicon strip tracker community joined this test using a custom-built sub-structure of the tracker (cf. Fig. 1), containing about 1% of the modules of the final CMS tracker. This structure was first tested at its assembly site (building 186 at CERN, referred to as building 186 in this note). It was then moved to the final location where the magnet and the other sub-detectors were set up for the challenge (site P5 on the LHC ring, referred to as P5 in this note).

A detailed description of the full silicon strip tracker can be found in [1]. The tracker setup used for MTCC consists of four layers: the 2 outermost layers are part of the final tracker outer barrel (TOB) and are labelled TOB L1 and TOB L5; the 2 innermost layers are part of the final tracker inner barrel (TIB) and are labelled TIB L2 and TIB L3. The TOB modules are placed on rods: there are six modules per rod, and two rods per TOB layer. The TIB modules are placed on strings: there are three modules per string, five strings on TIB L2, and 15 strings on TIB L3. All the modules in TIB L3, TOB L1 and TOB L5 measure precisely only position in $r - \phi$ plane (mono), whilst modules in TIB L2 can measure precisely also the z-coordinate (stereo). It is important to note that each layer is placed on an external or internal ring. This allows to have overlap (same layer) in the r-z plane between modules of internal and external rings (Fig 1 right). The overlap region is used during track reconstruction, both during the seeding procedure (Sect. 3.1) and during the pattern recognition (Sect.3.2). Some petals of disc 9 of the tracker end-cap (TEC) were present in the MTCC tracker setup but they were not used for track reconstruction and alignment because of the very low geometrical acceptance for cosmic muons crossing TEC and TIB (or TOB) modules simultaneously.

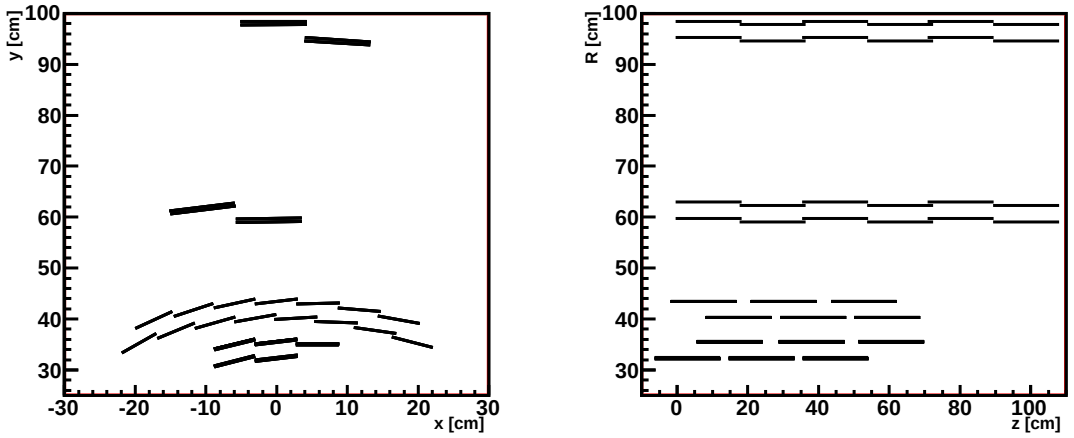

Figure 1: Custom-built sub-structure of the silicon strip tracker in (left) $x - y$ plane and in (right) $r - z$ plane.

Tracking, which is used to detect cosmic muons, is one of the fundamental tools to check the performance of both software and hardware of the tracker, and allows the alignment of layers and modules of the custom-built sub-structure.

This paper describes tracking and alignment algorithms, and presents the results of their application on data collected during MTCC. The data collected at P5 and building 186 and equivalent Monte Carlo simulations used for the analysis are summarised in section 2. The tracking algorithm and its performances on simulated data are the subject of section 3. Section 4 describes the preliminary alignment studies done before the tracker insertion in CMS at P5. In section 5, final alignment and tracking results on data collected at P5 with and without magnetic field are shown.

2 Data Samples

Three data samples were used in the studies described here. The first comes from simulation [2], while the two others contain real data collected respectively at building 186 and at P5. Monte Carlo simulations were performed

Monte Carlo			
Magnetic Field	# events	# events (hit layers ≥ 3)	# events (hit layers $= 4$)
$B = 0.0$ T	71402	6555	1366
$B = 4.0$ T	42460	3405	620
Data at Building 186			
Magnetic Field	# events	# events (hit layers ≥ 3)	# events (hit layers $= 4$)
$B = 0.0$ T	15811	8184	3824
Data at P5			
Magnetic Field	# events	# events (hit layers ≥ 3)	# events (hit layers $= 4$)
$B = 0.0$ T	6096	5962	1375
$B = 3.8$ T	3661	3552	510
$B = 4.0$ T	459	451	106

Table 1: Data samples divided in three sections: Monte Carlo simulations, data at building 186, and data at P5.

using a cosmic muon generator and a filter which requires that the muon has crossed both the tracker and the instrumented part of muon chambers used for trigger.

The number of events triggered and filtered are presented in table 1. The filter requires events with hits in at least two layers (first column), three layers (second column) and four layers (last column).

3 Tracking Algorithm

The tracking algorithm is essentially divided in three steps:

- **Seed creation**
  The first two hits of the track are selected and a preliminary trajectory is built.
- **Pattern recognition**
  At this step the hits compatible with track hypothesis are selected.
- **Fitting procedure**
  The hits are fitted in order to recalculate all the quantities of the track, such as direction, momentum and charge.

3.1 Seed creation

Seeding represents the phase devoted to finding the first segment of the tracks. In the case of MTCC the origin of the cosmics is such that an ad-hoc seeding has to be used with the respect to the standard one for the proton-proton collisions. For cosmic tracks the number of hits in the whole tracker are expected to be several orders of magnitude lower than in a p-p event. For this reason all the hit pairs which are geometrically compatible are considered as potential seeds. The definition of compatibility is the following one:

- The 2 hits are in neighbouring layers. In TIB region, where the overlap between modules of internal and external rings is about 5%, the hits can be in the same layer with the condition that one hit is in the internal and the other on the external ring.
- Stereo hits are not used for seeding since only one layer is equipped with this kind of module.
- The hit pair can be in the 2 layers of TOB, in the 2 layers of TIB, or in the overlaps of one of the 2 layers of TIB.
- The distance between the modules along z-axis is less than 30 cm (18 cm for seeds in the overlaps.)
- The distance between the x coordinate of the position of the hits is less than 2 times the distance in y. This because cosmics are expected to have small angles with respect to the vertical direction.

After selecting all the pairs, the initial trajectory is computed assuming that the preliminary direction is along the line connecting the two hits. All seeds that fulfil the previous selection criteria are considered in the pattern recognition. The final selection is done after the full track fit (Sect. 3.2) based on the quality of the trajectories.

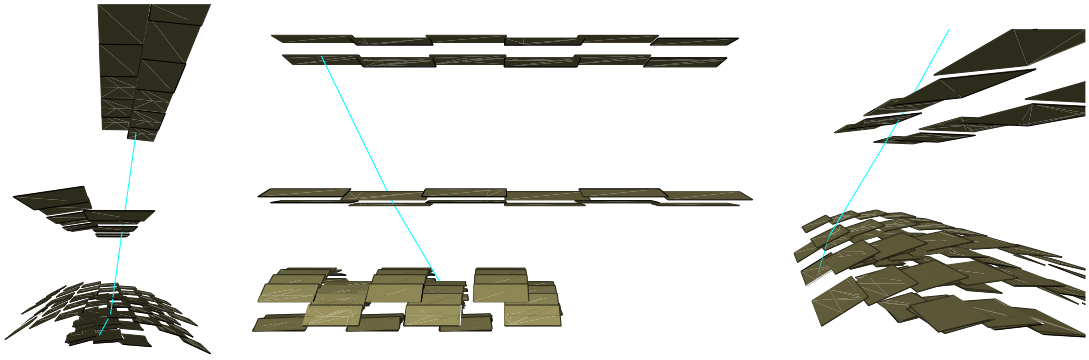

Figure 2: Examples of seeds in TIB layer1 and layer2 (left), in TOB layer1 and layer2 (center), in modules overlapping in TIB layer2 (right). Hits used to predict the first trajectory are in red.

3.2 Pattern recognition

The hit-selection algorithm is simplified with respect to the Combinatorial Kalman Filter [4] used in the proton-proton collisions. A seed, which comes from the previous step, can be at the top or bottom of the custom-built sub-structure of the tracker. If it is on the top (bottom), all the hits with a global y coordinate lower (higher) than the hit of the seed, are sorted in decreasing (increasing) order with respect to the vertical direction. The hits lining in the same layer but in different rings (overlap regions) are considered during this step. A very simple procedure establishes if the hit can be selected or not:

1. The trajectory is propagated to the surface of the hit module (the module on which the next ordered hit lies). Both possible charges of the muon are considered during the first propagation. Multiple scattering uncertainty is considered when the track is propagated. In absence of magnetic field the multiple scattering amount is evaluated considering $|p| = 2.5$ GeV which is the minimum value needed to trigger the muon in cosmic rays with the muon system.
2. The compatibility of the hit with the propagated trajectory is evaluated using a χ^2 estimator. (In the reconstruction of real data, the hit errors are inflated to take into account the alignment uncertainty.) The cut on the χ^2 is a parameter that can be set before starting to reconstruct the tracks. For this analysis a cut of $\chi^2 < 40$ was chosen.
3. If the hit is compatible, the trajectory is updated with the hit.

Finally the decision to discard or save a trajectory is based on the number of hits selected. For the MTCC this number was set to 3.

3.3 Fitting procedure

The fitting procedure is the same used from all the other CMS tracking algorithms and is based on the Kalman Filter [3]. Thus each trajectory is before fitted and then smoothed in the opposite direction. At the end of this phase several trajectories are still valid, but only one can be saved since only one track per event is expected.

For the MTCC, the best trajectory to be saved, is selected on the basis of the first criteria below, or if two trajectories are equally good, on the basis of the second or third criteria below:

1. The maximum number of layers with hits in the trajectory.
2. The maximum number of hits in the trajectory.
3. The minimum value of the χ^2,

All the quantities of the best trajectory are permanently stored: the hits used, the momentum and the position corresponding to the first and to the last hit, the charge, the value of the χ^2 and the covariance matrix.

3.4 Performance studies with simulated data

Angular and momentum resolutions, efficiency and fake rates were evaluated with Monte Carlo simulations. The energy spectrum of simulated cosmic muons is based on results of previous experiments [5], but available only above 2 GeV. In Fig. 3 the difference between simulated and reconstructed quantities (P_t, η and ϕ) are shown for all the tracks, for tracks that have reconstructed hits at least in 3 layers, and for tracks that have reconstructed hits in 4 layers. In table 2 the resolutions for these kinds of tracks are summarised. As expected the η resolution is much worse than the ϕ resolution because, there is only one layer measuring precisely the z coordinate of the hit. The case "all the tracks" has a worse resolution it contains a contribution from tracks with hits in 2 layers only.

Track quality	ϕ resolution [mrad]	η resolution	P_t relative resolution
All the tracks	1.8	0.14	10%
Hits in 3 layers	1.3	0.12	9%
Hits in 4 layers	1.0	0.07	6%

Table 2: Angular and energetic resolution of the cosmic track finder for different quality of the tracker.

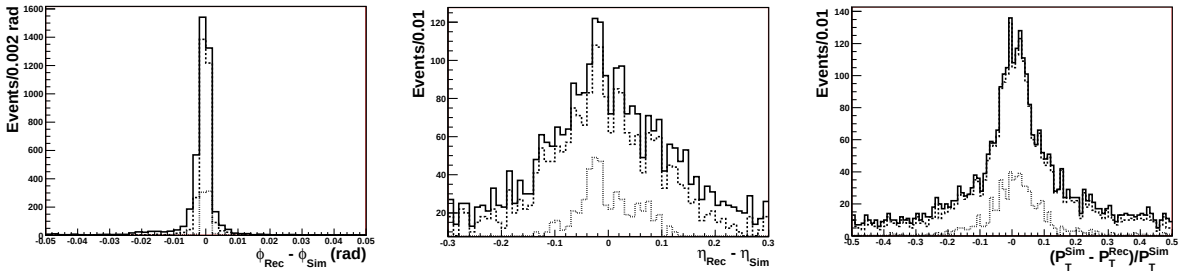

Figure 3: From left to right resolutions of ϕ, η, and the transverse momentum relative resolution. Resolutions are shown for all the tracks (solid), for tracks with hits at least in 3 layers (dashed) and for tracks that have hits in 4 layers (dotted).

In order to calculate tracking efficiency, only the events with a seed and 3 $r-\phi$ reconstructed hits correctly associated to a simulated hit created by the muon are considered. The seeding efficiency that was disentangled from the previous one is: 85% for category "all tracks", i.e. track with also hits in only 2 layers, 96% for track with hits in at least 3 layers and 99% for tracks with hits in 4 layers. Using the complementary sample (events with less than 3 hits correctly associated) the fake rate was calculated.

In Fig. 4 the efficiency is shown as a function of transverse momentum and for three different track qualities. The estimated fake rate is about 0.2%.

Another quantity that can be estimated with the simulation is the expected spatial resolution with a perfectly aligned detector. The plots in Fig. 5 and the results in table 3 have been obtained using the Monte Carlo sample with $B = 0.0$ T since all the alignment procedures will be run and tested with consistent data.

Modules	TIBL2 stereo	TIBL2 mono	TIBL3 mono	TOBL1 mono	TOBL5 mono
$\sigma_{\mathrm{residuals}}$ [μm]	270	40	37	68	155

Table 3: Standard deviation of the residuals from simulated data.

For each track crossing the modules, the distance between the reconstructed hit and the interpolated track position is computed. Since there is no contribution from misalignment, the residuals are only due to multiple scattering, intrinsic detector resolution and track interpolation. In particular the track interpolation contributes to the residuals in stereo modules of TIB layer 2 because of the poor resolution in the z direction, and in the outer TOB layer because it is placed far from the other layers of the MTCC structure. The residuals which are less affected from the track uncertainty, in TIB mono layers and TOB layer 2, are in good agreement with the residuals measured in several beam tests [1] that make use of an external telescope to measure the track directions. The values of the obtained residuals can be compared with the intrinsic detector resolution, which is of the order of 10 μm.

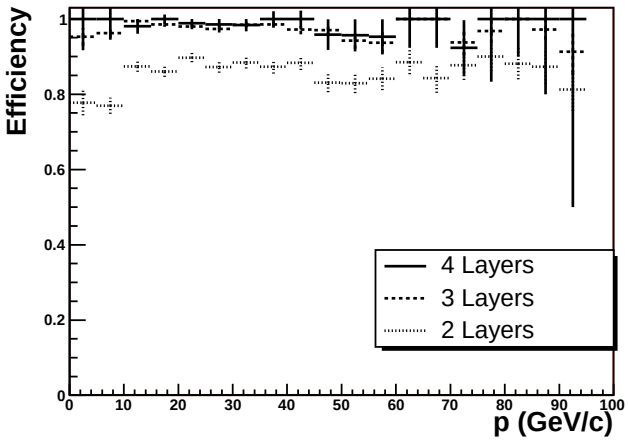

Figure 4: Tracking efficiency for all the tracks with hits correctly associated at least in 2, in 3, and in 4 layers.

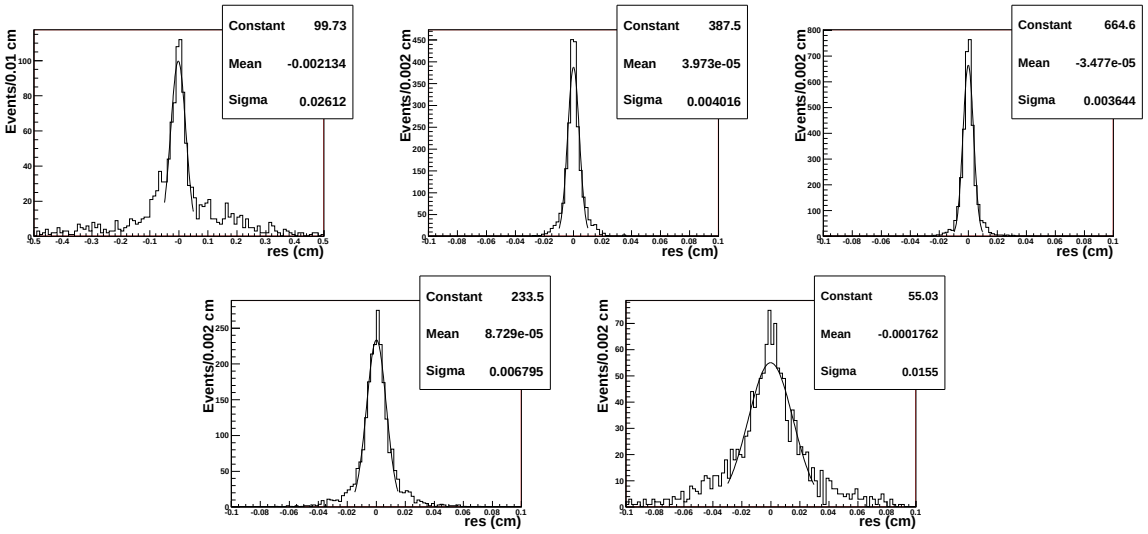

Figure 5: Residuals for (from left to right) stereo modules TIB L2, mono modules TIB L2, mono modules TIB L3, mono modules T0B L1, mono modules TOB L5.

4 Analysis of data collected at building 186

Preliminary tests of the data acquisition for the custom-built sub-structure of the silicon strip tracker were performed at building 186. At the same time, the full reconstruction chain (from raw data to tracks) has been tested.

The trigger scheme is shown in Fig. 6 and is based on three scintillators, one on the top of the structure ($S1$), one just below the TIB layers ($S2$), and one 1 meter below TIB layers ($S3$) with a small displacement in z with respect to the second scintillator. An event is selected if there is a signal in $S1$ and in one of the other two scintillators:

$$S1 \text{ AND } (S2 \text{ OR } S3) = \textit{true} \rightarrow \text{event selected}$$

This configuration was designed to optimise the trigger efficiency for cosmics crossing all the tracker layers.

4.1 Preliminary Alignment Study

In this section we present a method used to obtain a first set of alignment constants with the cosmic muon data. These constants allow the correction of the relative position between the four layers of the MTCC structure of the silicon strip tracker. The method is based on a stand-alone algorithm which uses only the hit position information in the transverse plane as shown on the right of Fig. 1.

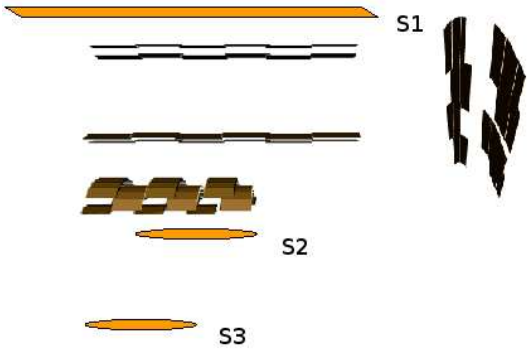

Figure 6: Trigger scheme at building 186.

In the first iteration of this algorithm, only the relative position between TIB and TOB layers that can be parameterized with two translations in the x (dx) and y(dy) directions and one rotation around the longitudinal axis ($d\phi$), was determined. These three quantities refer to the global corrections to be applied at the TIB position.

As shown by table 1 during the MTCC preparation data was taken without magnetic field, allowing a reconstruction of straight tracks with a simple linear fit. For the preliminary alignment study, only events with hits in all the layers (3155 events in total) were considered.

The distribution of residuals (Fig. 9, left) in TIB layers shows a double-peak structure, which is the most evident effect of the rotation of the TIB layers with respect to TOB. In order to correct this effect, the difference in slope between segments built in TIB and TOB layers is reconstructed for each track. The Gaussian fit to the distribution of $\Delta_\phi = \phi_{TIB} - \phi_{TOB}$ (Fig. 7) was used to evaluate $d\phi$(See Table 4). After rotating the TIB structure of 60 mrad

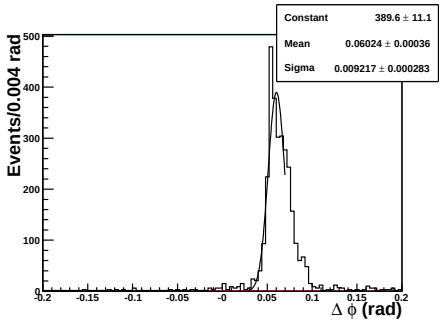

Figure 7: Distributions of Δ_ϕ between segments in TIB and TOB.

the double peak structure disappears and the corrected distribution of the residuals is the one shown in the center of Fig. 9

$\langle\Delta\phi\rangle$ (rad)	0.06024±0.00036
$\sigma_{\Delta\phi}$ (rad)	0.00922 ± 0.00028

Table 4: $d\phi$ from the Gaussian fit to the difference in slope between TIB and TOB.

The evaluation of the constant dx for TIB layers can be obtained by defining a χ^2 variable (eqn. 1), which is closely related to the sum of the residuals of the linear fit. From the minimisation of χ^2, dx and dy are determined in two separate steps.

$$\chi^2 = (d2^2 + \sigma_{d2}^2) + (d3^2 + \sigma_{d3}^2) \tag{1}$$

where $d2$ (resp. $d3$) and σ_2 (resp. σ_3) are the mean and width of the distribution of residuals between TOB tracks and TIB2 (resp. TIB3) hits, obtained from a Gaussian fit to these distributions.

Fig. 8 shows how the χ^2 depends on dx, displaying a minimum around -4 cm. After finding the value of dx,

the same procedure is applied to measure dy. The results from the minimisation are summarised in table 5. After applying the corrections related to the translations are shown in Fig. 9, in which the distributions of the residuals, as expected, are centred around 0 with a width of about 1 mm.

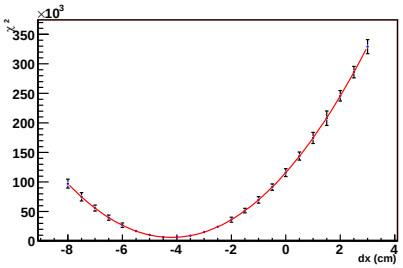

Figure 8: χ^2 variable as a function of dx.

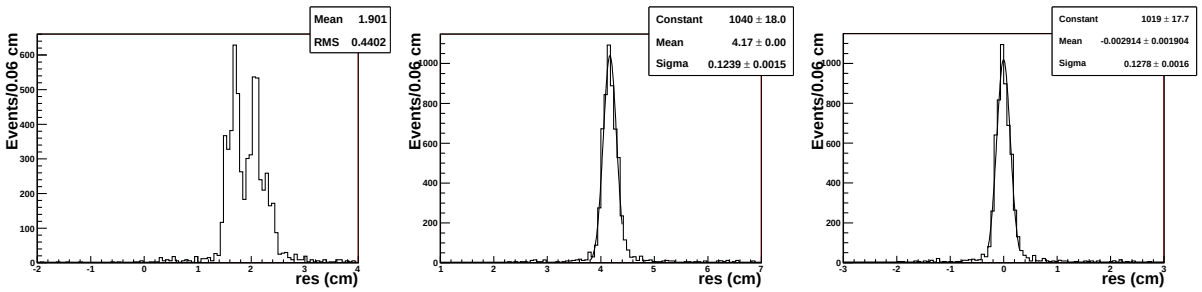

Figure 9: TIB residual before any corrections(left), after rotation (centre), after rotation and translations(right)

dx [cm]	-4.188 ± 0.012
dy [cm]	0.082 ± 0.014

Table 5: Translation of TIB with respect to TOB. The results are obtained minimising the χ^2 variable.

4.2 Effect of preliminary alignment on tracking

In order to evaluate the effect of the preliminary alignment on tracking, data acquired at building 186 was reconstructed before and after applying the alignment corrections.
The number of reconstructed tracks increases from 952 to 2526 (+ 165 %) and also the spatial resolution, as shown by the residuals in TOB L5 in Fig. 10 is much better.

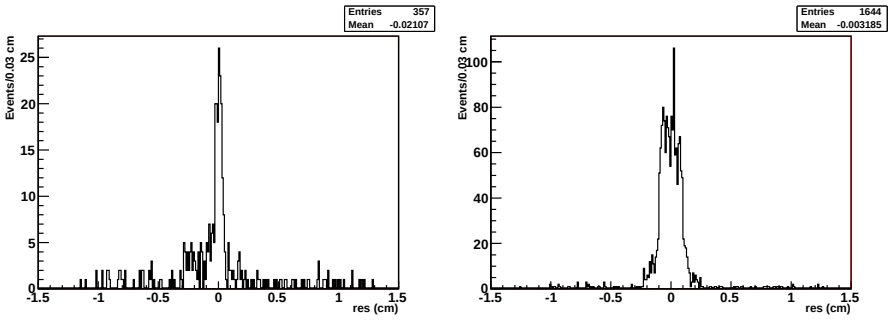

Figure 10: Residuals in TOB L5 before (left) and after applying the preliminary alignment corrections.

4.3 Module alignment sensitivity

The aim of this study is to estimate the sensitivity of cosmic data to the local position of individual modules, using overlap in TIB layers. The layout of TIB presents an overlap in z direction which was introduced both to increase the efficiency and to allow relative sensor alignment. The small lever arm between these layers provides an adequate resolution and good sensitivity to sensor positions.

Only the events in which one hit is found in TIBL2 and two hits in TIBL3 were selected. The estimator used for module alignment is the residual between the track segment from TIBL2 hit and TIBL3 outermost hit, and the TIBL3 innermost hit $D_{ov} = x_{(L2,L3out)} - x_{L3in}$. Fig. 11 shows the distribution of D_{ov} after global preliminary alignment has been applied. It has a width of about 200 μm and is clearly displaced from zero. This can be corrected by introducing different global parameters for the internal and the external sub-layers of TIBL3. By minimising the sum of the residuals squared, we obtain a shift of 1.2 mm for the TIBL3 outermost layer with respect to the innermost one.

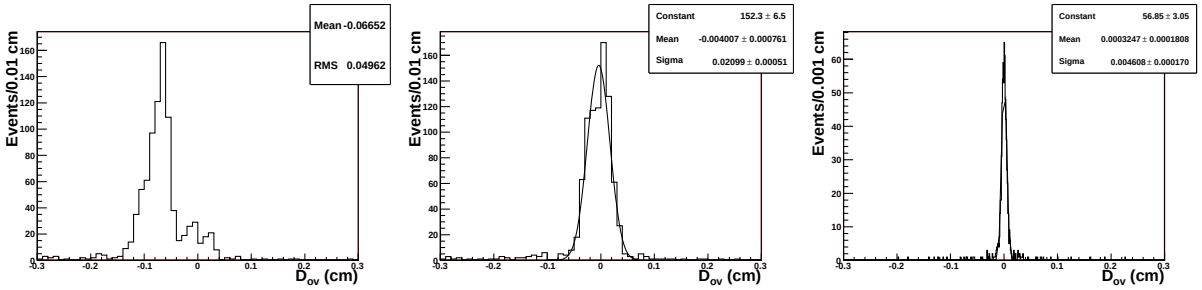

Figure 11: D_{ov} distribution after the global preliminary alignment (left), after moving the external TIB L3 (centre), after correcting locally (right).

Fig. 12 shows the dependence of residual with respect to the x position of the TIBL3 innermost hit. In order to study the single module positions, triplets from overlapping modules are selected in 21 different regions, 7 in ϕ and 3 in z. Fig. 13 (black) shows the correlation between the residual and the track direction for some of these regions: the offset of the residual is related to the module shift ΔX_{loc} in the direction perpendicular to readout strips, while the slope of the distribution is related to the module shift ΔZ_{loc} in the direction perpendicular to the sensor plane. The sums of the residuals squared are minimised for each of the 21 modules, with respect to ΔX_{loc} and ΔZ_{loc}: the residual distribution is shown in Fig. 13 (gray) after this local corrections.

From the width of this distribution, which is about 45 μm (Fig. 11 right), and correcting for the geometrical factor from extrapolation, the estimated point resolution (which includes all the residual effects from mis-alignment,

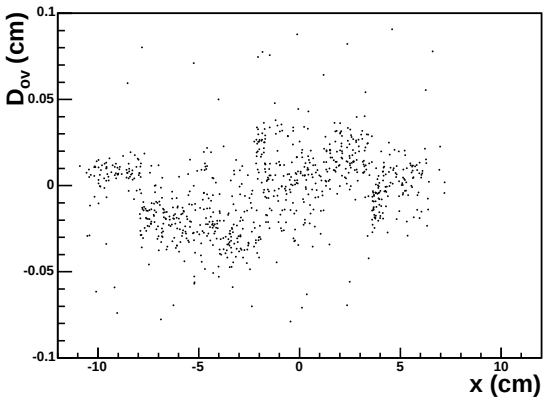

Figure 12: Dependence of the residual on the x position.

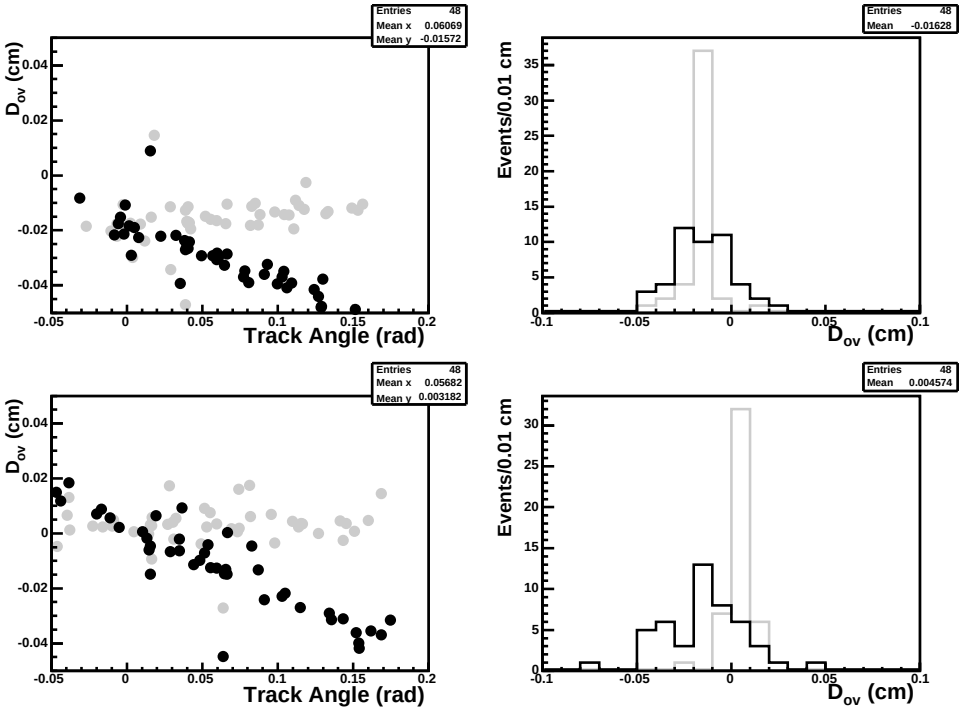

Figure 13: Dependence of the residual on the track direction. For two different module triplets, the dependence of the residual on the track angle (left) and their distribution (right) are shown before (black) and after (gray) the local correction.

multiple scattering and intrinsic resolution) is infered to be about 30 μm.

5 Analysis of data collected at P5

Data collected at P5 was triggered by the muon system [6] of CMS, especially by the Drift Tubes in the barrel region and, to a lesser extent, by the Cathode Strip Chambers in the end-cap.

5.1 Survey measurements of MTCC structure

TIB

A set of survey measurements was made on the structures of the of the MTCC TIB to determine the sensor centre position and orientation. These data are used as input for the alignment algorithms and track reconstruction.

Measurements on TIB layer structures were performed, before modules were mounted, using a DEA measurement machine [7] with a touch-trigger probe capable of measuring the coordinates of up to 2000 points in three hours with accuracy better than 50 μm. A cylindrical reference frame, similar to the CMS one, was defined for each layer structure by measuring the coordinates of the surface of the bushes placed on each layer flange. Then for each module location a set of measurements and operations was done in order to retrieve the orientation of the ledge plane (where the modules are screwed) and define a local right-handed reference frame, according to the CMS simulation and reconstruction framework [8]. The orientation of each ledge plane is defined by the normal to its surface, and to a good approximation corresponds to that of the sensor. The directions in each ledge plane parallel and perpendicular to the micro-strips were measured and used to determine the coordinates of the centre of the sensor.

The position of the sensor centre is compared with the expected values. The mean and RMS of the distributions of the residuals between the measured and expected values of the z coordinate are shown in Table 6.

The bigger difference in z for the MTCC TIB Layer 2 is due to the *ad-hoc* structure used, which is not a carbon fibre semi-cylinder as for the corresponding Tracker layer.

MTCC TIB		$z^{measured} - z^{design}$ [mm]	
Layer	Part	Mean	RMS
2	int	-0.476	0.074
2	ext	-0.009	0.141
3	int	$+0.126$	0.057
3	ext	-0.199	0.062

Table 6: Residuals between the measured ($z^{measured}$) and design (z^{design}) position of sensor centres along z direction for the internal and external surfaces of the MTCC TIB layers.

The distribution of the polar radius, defined as the radial distance from the axis $x = y = 0$ of the $r\varphi$ sensor centres, is shown in Figure 14 for the internal part of the MTCC TIB Layer 3 modules.

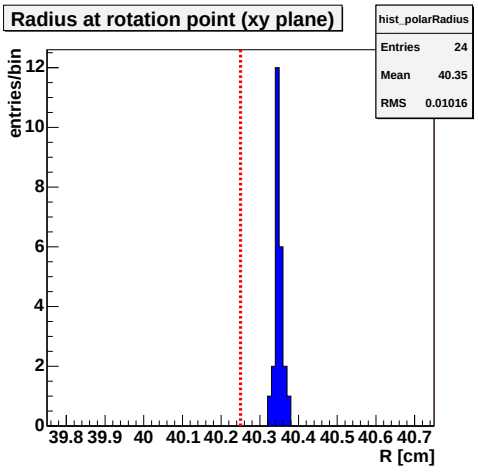

Figure 14: Polar radius distribution for the $r\varphi$ sensors of the internal strings of the MTCC TIB Layer 3. Three modules per string are mounted. The horizontal dashed line represents the design value of the polar radius.

The value of the mean and RMS of the polar radius distribution for each MTCC TIB Layer with the $r\varphi$ module design values are summarised in Table 7.

MTCC TIB		Polar Radius [mm]			
Layer	Part	Measured	RMS	Design	Measured−Design
2	int	319.6	0.03	321.9	-0.23
2	ext	354.1	0.07	356.1	-0.20
3	int	403.5	0.01	402.5	+0.10
3	ext	435.2	0.02	434.5	+0.07

Table 7: Measured value and distribution spread of the the MTCC TIB layer cylinder polar radius compared with the design value. The polar radius is measured in the $x - y$ plane the axis $x = y = 0$ of the $r\varphi$ sensor centre.

The string tilt angle, defined as the angle between the normal to the sensor plane and the radial direction in $x - y$ plane, is expected to be 9°. The measurements summarised in Table 8 are compatible with the design value.

TIB+		Tilt Angle [deg]			
Layer	Part	Measured	RMS	Design	Measured−Design
2	int	8.72	0.19	9	-0.28
2	ext	10.36	0.17	9	+1.36
3	int	8.79	0.18	9	-0.21
3	ext	8.74	0.27	9	-0.26

Table 8: Measured value and distribution spread of the the MTCC TIB ledge plane tilt angle compared with the design value.

TOB

For all the TOB rods, the location and orientation of the precision pins that determine the position of the modules in the rod, was measured in the rod frame assembly site, for all rod frames. Such data have been analysed and translated to an expected displacement and misalignment of the modules with respect to the ideal rod reference frame, obtaining a spread in the precise coordinate of 30 μm. The real relative displacement of the sensors in a rod also includes contributions from the spread in the positioning of the sensors on the module frame (typically of the order of 10 μm), the precision of the elements of the frame clamping the pins (not known), and possible deformations of the pins during the module mounting operation (also not known), which could actually modify the pin geometry. It is therefore not obvious a priori that the data from the survey of the pins are valid as pre-alignment constants for the rods. The first high-precision alignment exercise carried out with TOB rods, using the Cosmic Rack setup, shows no correlations between the pin survey data and the alignment constants derived from tracks. There is therefore no evidence, so far, that those data should be used [9].

5.2 Alignment analysis

The CMS software alignment framework was used to align the data collected at P5. The final alignment was obtained using the Hits and Impact Points algorithm (HIP) [10], together with construction information for movements at sensor level, as described in the previous section.

The alignment framework indeed offers the possibility to add construction information as a starting point for the algorithm. This information was converted into a database object that was read in by the alignment algorithm. (The corrections reported in Sect. 4, however, were not used in this analysis.)

The HIP algorithm determines the sensor alignment by minimising a local χ^2 function: it does not explicitly take into account correlations between sensors. These are taken care of implicitly by iterating over the full event sample. The HIP algorithm is computationally light and was already successfully applied to the silicon tracker alignment in Monte Carlo simulations.

In this study, however, alignment at sensor level is made difficult by the small number of hits per sensor. The alignment was, therefore, only performed at the level of TOB rods and TIB strings. In addition, the setup itself is not optimal from the alignment point of view, especially for the TOB: small number of layers, limited range of track angle and large lever arm in TOB. The alignment was then done in two steps: 1) alignment of TOB rods with

TIB fixed, assuming the TIB misalignment is small enough compared to the TOB, thanks to survey information; 2) alignment of TIB strings with TOB fixed to its aligned position. Note that, as a consequence, the result of TIB alignment cannot be easily compared with survey information, the two providing measurements at different levels.

The degrees of freedom of TIB strings and TOB rods are defined in their local (u,v, w) frame: the u axis is perpendicular to the strips (approximately collinear to the global x axis); the v axis is parallel to the strips (approximately collinear to the global z axis); the w axis is normal to the strips (approximately collinear to the global y axis). The 6 alignment parameters are then: shifts along the u, v and w axes, and rotations around the same (labelled α, β and γ, respectively). Detailed studies showed that only a subset of the parameters could be aligned, due to the particular geometry of this setup and the nature of cosmic muons. Since u is the measured coordinate, it was always well constrained. The same is true for γ. There was no constraint on α since it has almost no impact on the sensitive coordinate u, and the angle β only affects it to second order, in the case of vertical tracks.

The algorithm was run on the full data sample acquired without magnetic field. As shown in Table 1, this sample is indeed significantly larger than the one with magnetic field. In order to increase the track efficiency in the first iterations, an alignment position error (APE) of 3.5 mm is added in quadrature to the hit position error, linearly decreasing to 0 mm in 10 iterations. The size of this error corresponds to the size of the largest movements measured by the survey. It turned out to be significantly smaller than the misalignment found in TOB rods. The APE, however, also increases fake rates and biases the track fit. Our choice is a trade-off between the two effects of the APE, and was also justified *a posteriori* by the good convergence of the algorithm.

In the first step, the alignment of TOB rods, the free parameters are u shifts and γ rotations; w shifts could not be constrained because tracks crossing TOB rods are almost vertical. The convergence of the global positions of the TOB rods is illustrated on Fig. 15. The aligned position is reached after 210 iterations (only the 210 first of 250 iterations in total are shown on the figure). The two groups of rods visible in the u shifts correspond to coherent movements of the two TOB layers.

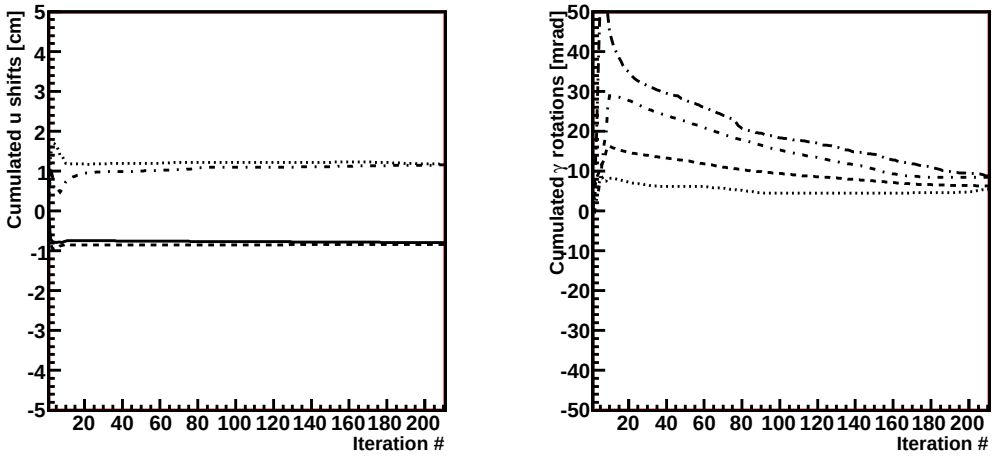

Figure 15: Shifts in the local u coordinate (left) and γ rotations (right) of the 4 TOB rods with respect to the initial position, as a function of the iteration number.

In the second step, the alignment of TIB strings, the free parameters are the u and w shifts, and the γ rotation. In this case, w can be constrained by non-vertical tracks, thanks to the good ϕ coverage of TIB. The starting configuration is the outcome of the previous step. The convergence is illustrated on Fig. 16. Seven strings in TIB layer 3 were not hit often enough to be used in this alignment and were kept fixed. The two groups of strings in the w shifts correspond to coherent movements of the two TIB layers.

As an additional convergence test, we have run TOB alignment again and checked that we obtain movements compatible with the alignment sensitivity in u and v. We also run the same procedure without using the survey information. The convergence of the TIB strings alignment was then significantly slower (more than 100 iterations were needed) and the coherent movements were not visible anymore.

The shifts and rotations applied by the algorithm are summarised in Table 9.

Alignment corrections were saved in database objects and used in an analysis of the residuals in the different

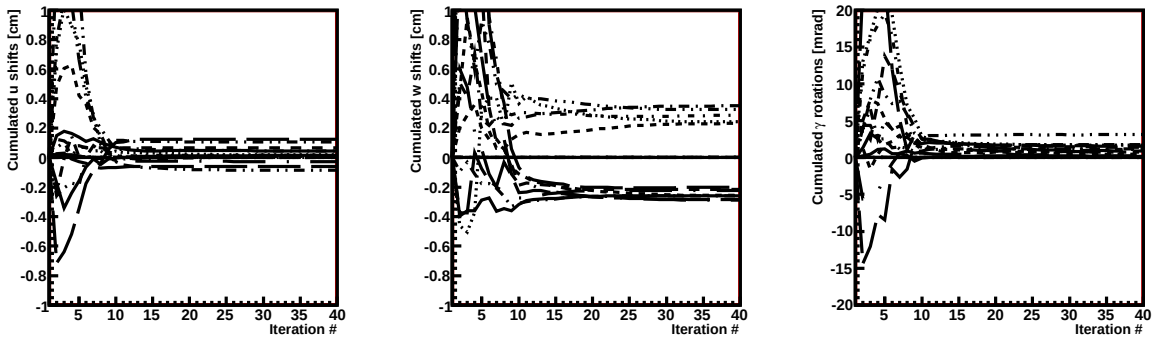

Figure 16: Shifts in the local (left) u and (middle) v coordinates, and (right) γ rotations of the TIB strings with respect to the initial position, as a function of the iteration number.

	$\langle\Delta u\rangle$ [mm]	$\langle\Delta w\rangle$ [mm]	$\langle\Delta\gamma\rangle$ [mrad]
TOB	9.91	N/A	7.2
TIB	0.31	1.7	0.76

Table 9: Summary of average local shifts applied to the sub-structures of TIB and TOB.

layers of the tracker. This was done on the dataset at P5 without magnetic field. In order to account for remaining misalignment, the hit error was inflated by 100 μm. The quality of track reconstruction is then estimated by the number of reconstructed tracks, the average χ^2, the average number of hits per track and the spatial resolution. The results are summarised in Table 10, before alignment, after preliminary alignment and after the alignment described in this section (without and with survey information).

Alignment status	# rec. tracks	$\langle\chi^2\rangle$	$\langle$#of hits$\rangle$	res. TIBL2 mono [μm]	res. TIBL3 mono [μm]	res. TOBL1 mono [μm]	res. TOBL5 mono [μm]
No alignment	1460	20.1	3.3	526	416	2660	1986
Prel. alignment	3263	16.5	4.0	518	387	1547	1999
Alignment w/o survey	4894	6.5	4.3	208	135	389	710
Alignment w/survey	4956	6.0	4.3	177	125	357	687

Table 10: Most sensitive track quantities for three different alignment conditions. All the numbers are evaluated for tracks with hits in 3 or more layers.

The distributions are represented in Fig. 17. A clear improvement of the track quality after alignment is observed. Remaining structures can still be observed in the residuals (especially in TIB layer 3), due to unaligned strings or misalignment of modules on strings and rods. TOB layer 5 residuals are still large, as can be expected from the 40 cm lever arm between this layer and the closest layer. The input of survey measurements clearly improves the quality of track reconstruction by adding individual module information.

All the following plots and results were obtained using the results of the HIP algorithm, with the hit error inflated by 100 μm. This corresponds to the expected mounting precision of modules on strings and rods, while alignment was done at string and rod level. The distributions of the most important quantities of the tracks reconstructed with the cosmic track finder are displayed respectively for $B = 0.0$ T in Fig. 18 and for $B = 3.8$ T in Fig. 19. The number of reconstructed tracks with hit in at least two layers ("all tracks") after the alignment is 5163 for the case $B = 0.0$ T, 3367 for the case $B = 3.8$ T and 421 for the case $B = 4.0$ T.

The ϕ distributions for the three different values of magnetic field have a peak around $-\pi/2$, as expected, and the η distributions are compatible with the trigger layout.

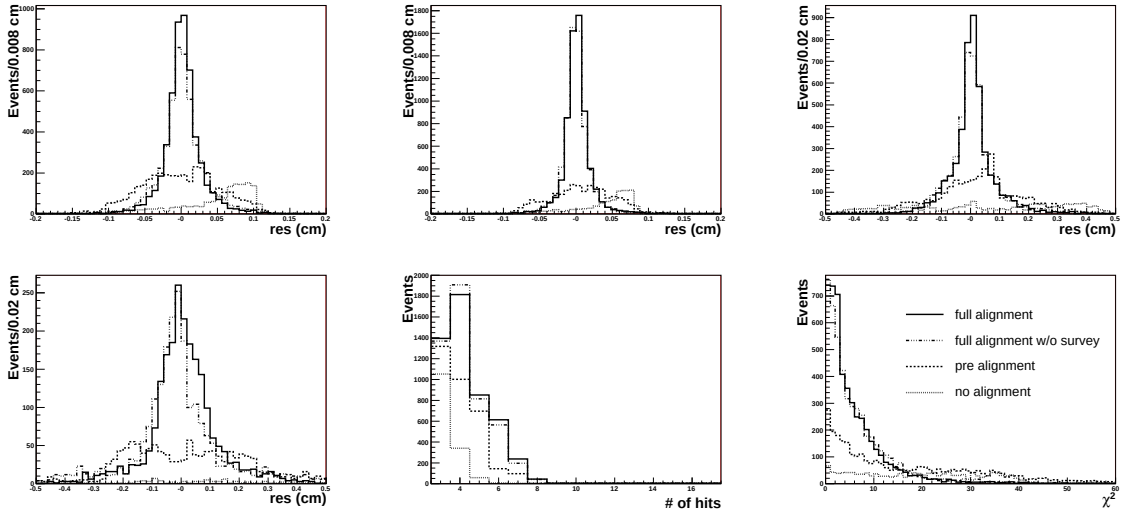

Figure 17: Hit residuals in (top left) all TIB layer 2 modules, (top middle) TIB layer 3, (top right) TOB layer 1 modules, (bottom left) TOB layer 5 modules, (bottom middle) number of hit and (bottom right) track χ^2. The distributions without alignment, with pre-alignment, with full alignment without survey and with full alignment with survey are compared.

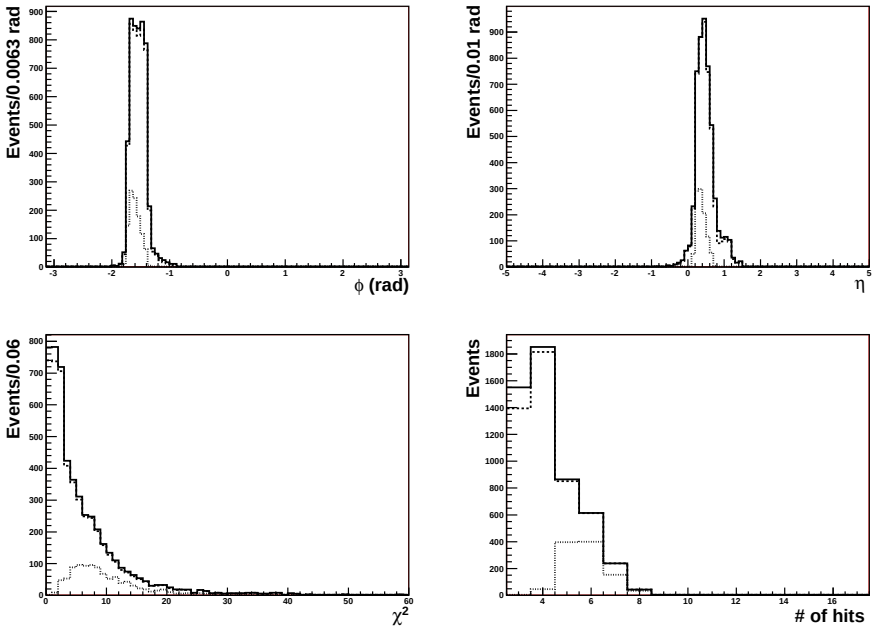

Figure 18: Distributions for the sample collected with $B = 0.0$ T of ϕ direction (top-left), η direction (top-right), χ^2 (bottom-left), number of hit (bottom-right). All the distributions are shown for all the tracks (solid), for tracks with hits at least in 3 layers (dashed), and for tracks with hits in 4 layers (dotted).

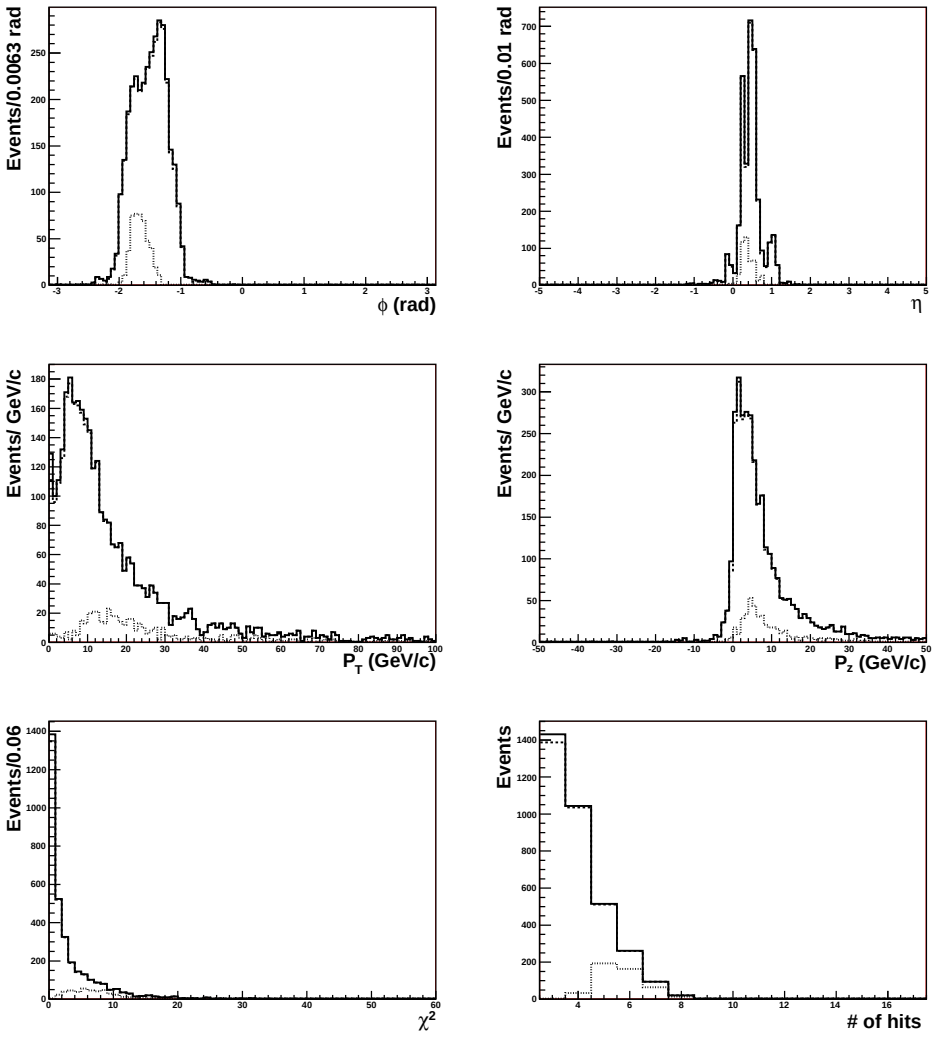

Figure 19: Distributions for the sample collected with $B = 3.8$ T of ϕ direction (top left), η direction (top middle), transverse momentum (top right), longitudinal momentum (bottom left), χ^2 (bottom middle), number of hit (bottom-right). All the distributions are shown for all the tracks (solid), for tracks with hits at least in 3 layers (dashed), and for tracks with hits in 4 layers (dotted).

5.3 Muon chambers vs Tracker

The last goal of the test, from the reconstruction point of view, is the comparison of the tracks reconstructed by the tracker with tracks reconstructed by the muon chambers. For both tracker and muon drift tubes the momentum and the direction was calculated at the point when the cosmic muon enters inside the sub-detector (See fig. 20), under the hypothesis that cosmic rays come from the top of CMS.

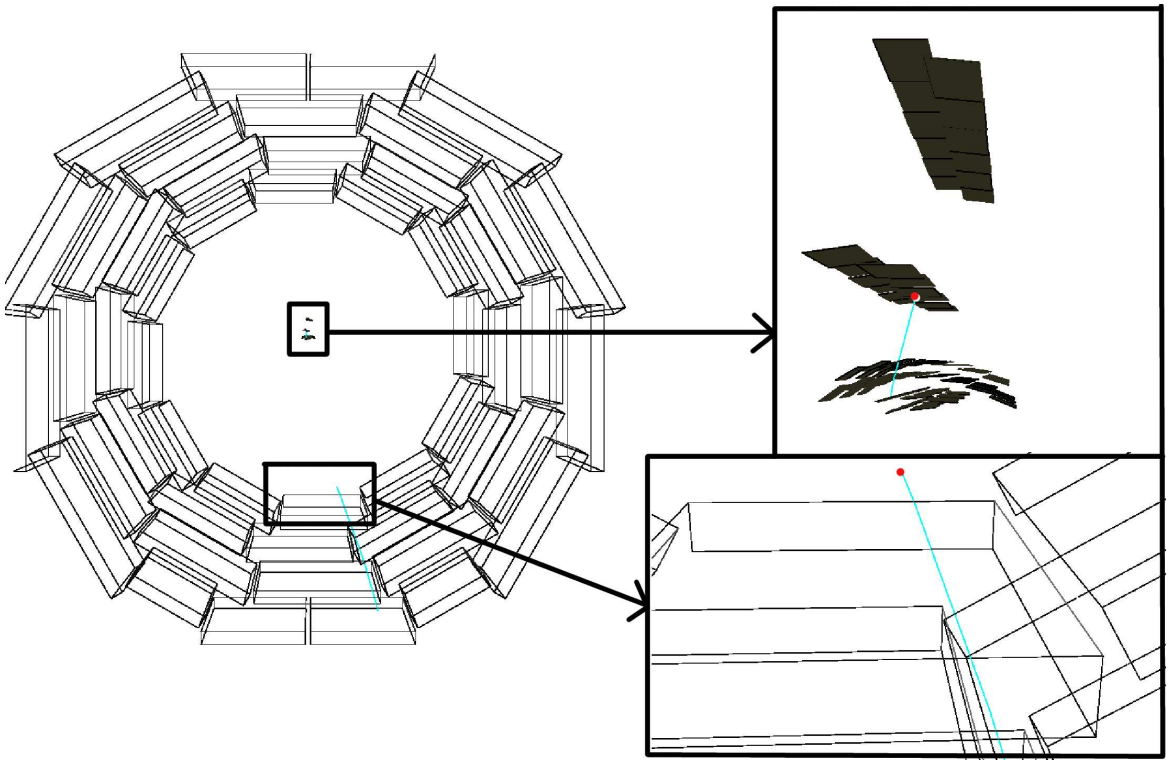

Figure 20: Section of tracker and Drift Tubes. On the right the points (red) where the muon enters in the sub-detectors and the track quantities are calculated, are shown. Tracks are drawn in light blue.

Figure 21 shows the correlation of the direction measured in absence of magnetic field. The correlation on the direction in the transverse plane is very good and the width of the distribution of $\phi_{tk} - \phi_{DT}$ is about 25 mrads. As expected, the poor resolution in η direction is the cause of the big spread in η correlation, which is significantly improved after selecting tracks with hits in all the layers.

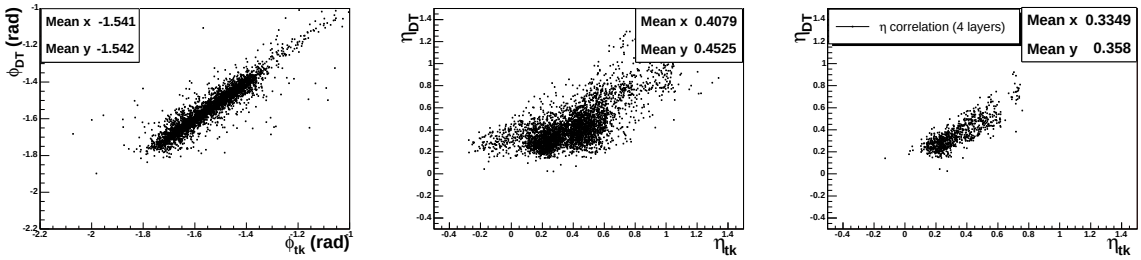

Figure 21: Correlations of directions of tracks, in absence of magnetic field, reconstructed in the tracker and the ones reconstructed in the drift tubes. On the left the ϕ correlation is shown, while on the centre (right) plot there is the η correlation for all the tracks (for tracks with hits in 4 layers).

For events with the magnetic field switched on, studying the correlation in the transverse plane is more difficult since tracks bend. The difference of $\phi_{tk} - \phi_{DT}$(fig. 22), as expected, decreases with increasing transverse momentum and has different sign for positive and negative muons. There are several sources for the spread of this plot, like the resolution of transverse momentum in the tracker and the different path length of the cosmic muon between tracker and drift tubes.

The η correlation behaves as for tracks reconstructed with $B = 0.0$ T.

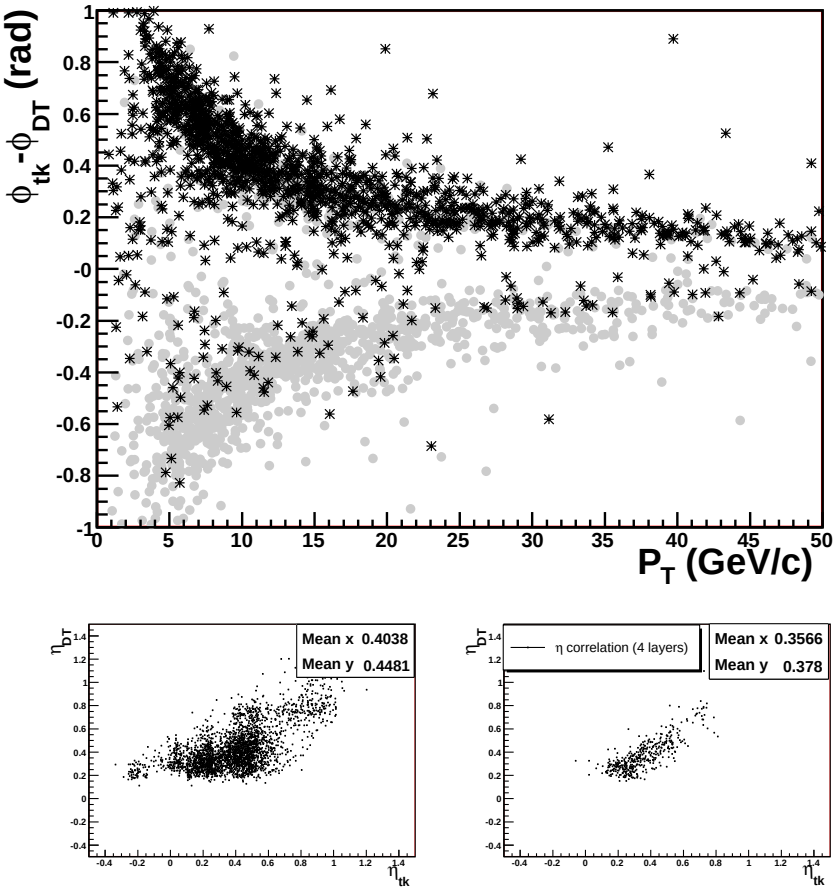

Figure 22: Correlations in the direction of tracks, as reconstructed in the tracker or in the drift tubes, for B = 3.8 T. On the top the difference $\phi_{tk} - \phi_{Dt}$ is correlated to the transverse momentum measured by the tracker for positive (black) and negative (gray) muons. On the bottom left (right) plot the η correlation for all the tracks (for tracks with hits in 4 layers) is shown.

6 Conclusions

The algorithm used to reconstruct tracks associated to cosmic muons in MTCC has been described. The algorithm is fully efficient for tracks that cross all the layers and has a very good angular resolution (1-2 mrad in ϕ). For muons with energy larger than 2 GeV, the momentum resolution is around 10%.

The sample of cosmics acquired at building 186 was analysed and a first set of alignment constants was found, which significantly improved the tracking efficiency (+160$\%$) and spatial resolution. The sensitivity to the local alignment in the TIB layers was investigated. The method, based on the overlaps, reached a spatial resolution of 30 μm.

Data were collected at P5 with 3 different values of the magnetic field, namely 0.0 T, 3.8 T and 4.0 T. The CMS alignment software was used to align the silicon strip structure with these data, using survey information from the construction as a starting point for corrections to the TIB strings. The final corrections significantly improved the track quality: we observed an increase by a factor 2.4 in the number of reconstructed tracks, a significant decrease of the track χ^2 and a reduction of the residuals to a level of hundreds of micrometres. The use of survey measurements was shown proved to be beneficial.

The tracks reconstructed, after the alignment corrections, show the expected angular distributions, and are compatible with tracks reconstructed in the muon system.

References

[1] CMS collaboration, *The Tracker Project Technical Design Report*, **CERN-LHCC-98-06** (1998) and the *addendum* **CERN-LHCC-2000-016** (2000).

[2] D.Abbaneo *et al.*, *Tracker Operation and Performance at the Magnet Test and Cosmic Challenge*, **CERN-CMS-NOTE-2007-029**.

[3] R. Fruhwirth, *Application Of Kalman Filtering To Track And Vertex Fitting*, Nucl. Instrum. Meth. A **262** (1987) 444.

[4] W. Adam, B. Mangano, T. Speer and T. Todorov, *Track reconstruction in the CMS tracker*, **CERN-CMS-NOTE-2006-041.**

[5] T. Djemil, R. Attallah and J. N. Capdevielle, *Simulation of the atmospheric muon flux with CORSIKA*, Int. J. Mod. Phys. A **20** (2005) 6950.

[6] CMS collaboration, *The Muon Project Technical Design Report*, **CERN-LHCC-97-32.**

[7] DEA Hexagon Metrology, see *http://www.dea.it*.

[8] M. Winkler, dissertation Technischen Universitat Wien, Fakultat fur Technische Naturwissenschaften und Informatik, Wien, Austria, *"A Comparative Study of Track Reconstruction Methods in the Context of CMS Physics"*,**CMS-THESIS 2002-015**.

[9] T. Lampén, V. Karimäki, S. Saarinen and O. Buchmüller, *Alignment of the cosmic rack with the hits and impact points algorithm*, **CERN-CMS-NOTE-2006-006.**

[10] V. Karimäki *et al.*, *The HIP Algorithm for track based alignment and its Application to the CMS pixel detector*, **CERN-CMS-NOTE-2006-018.**